Nitrogen-rich activated carbon monoliths *via* ice-templating with high CO_2 and H_2 adsorption capacities

Received 00th January 20xx,
Accepted 00th January 20xx

DOI: 10.1039/x0xx00000x

www.rsc.org/

Aled D. Roberts,[a,b] Jet-Sing M. Lee,[a] Siew Yee Wong,[b] Xu Li*[b,c] and Haifei Zhang*[a]

Hierarchically porous, nitrogen-rich activated carbon monoliths were prepared *via* ice-templating, carbonization and chemical activation of a polyacrylonitrile (PAN) precursor. Ice-templating of the PAN provided a rigid macroporous polymer scaffold, into which the chemical activating agent KOH was infused, prior to oxidative annealing, carbonization and activation. By varying the amount of KOH infused, the surface areas and N contents of the activated carbons could be varied. This allowed tuning of the materials to favor either CO_2 or H_2 uptake – where the optimized material for CO_2 adsorption had a BET surface area of 1049 $m^2 g^{-1}$, an N content of 14.9 wt. %, and a CO_2 adsorption of 16.12 mmol g^{-1} at 298 K and 10 bar. The optimized material for H_2 uptake had a BET surface area of 2206 $m^2 g^{-1}$, an N content of 1.29 wt. %, and a H_2 adsorption of 2.66 wt. % at 77 K and 1.2 bar. These high CO_2 and H_2 adsorption values are achieved despite the relatively facile ice-templating process and the use of the commercially available polymer precursor PAN without further chemical modification.

1. Introduction

With a clear causal link between anthropogenic CO_2 emissions and global warming, there is growing urgency for countries to slash greenhouse gas emissions to mitigate the worst effects of climate change. A viable short-term solution to meet CO_2 emission reduction targets is carbon capture and storage (CCS) from large point-sources such as power stations, refineries and cement-manufacturing facilities.[1-3] The development and deployment of CCS technologies is hampered however by high costs and systematic inefficiencies; with the energy requirements alone increasing 25-40 % for plants employing conventional 'amide scrubbing' CCS technologies.[2] There is therefore a clear need for technological advances – mainly in the form of new, low cost materials with high and reversible CO_2 adsorption – to improve efficiency and drive down costs to enable CCS technology to be widely adopted. Transitioning away from petroleum-based automotive transport to low-carbon alternatives is also a huge priority for CO_2 emission reduction – with petroleum supplying ~95 % of energy for transport and accounting for approximately 23 % of global CO_2 emissions.[4] Replacing internal combustion engines with H_2 fuel cells is one option which may achieve this goal, however the development of materials capable of storing significant quantities of H_2 remains a challenge.[5]

Various high surface area porous materials, such as metal-organic frameworks (MOFs),[6,7] covalent organic frameworks (COFs),[8] zeolites,[9] microporous polymers[10] and activated carbons (ACs),[11-14] can adsorb and desorb gases such as CO_2 and H_2 through pressure or temperature swing cycles, and are being actively investigated for their utilization in CCS and H_2 storage technology. Of these, ACs hold important advantages over alternatives, including high thermal and chemical stability, relative ease and low cost of manufacture, as well as wide diversity and availability of precursors.[11] Such carbons can also possess extremely versatile properties which can be tuned depending on the manufacturing conditions or choice of precursors; including the morphology, crystallinity, microstructure, porosity and pore-size distribution, as well as heteroatom-doping and surface functionalization.[11,15]

Since the adsorption of gases occurs *via* their physical interaction with the AC surface, high surface areas generally lead to higher gas adsorption. With regards to CO_2 sorption, it has been proposed that a combination of micro- (< 2 nm), meso- (2 – 50 nm) and macropores (so called *hierarchical* porosity) can lead to superior CO_2 adsorption than purely microporous ACs due to multilayer adsorption within the larger pores.[16] A hierarchical pore structure may also facilitate relatively fast sorption kinetics,[17] since small and convoluted pore structures of a purely microporous material would impede diffusion of gases to and from the AC surfaces. As reported in the use of liquid amine solvents for CO_2 adsorption,[18] nitrogen-doping of the carbon can also significantly increase the CO_2 adsorption in relation to non-doped carbons.[17, 19-21] The enhancement in CO_2 adsorption has been widely reported to be the affinity between the acidic CO_2 molecules and the basic lone pair of electrons on N leading to stronger bonding interactions.[17] However, Qiao and co-authors attributed the excellent CO_2 capture capacity of their carbons to hydrogen bonding interactions between hydrogen atoms (from CH and NH) on the carbon surface and CO_2 molecules, which is strongly facilitated by the presence of N atoms in the carbon.[22] Although different forms of N may be available in carbon materials, the contributions of these N-containing groups have not been investigated in details. In a recent modelling study via a density functional theory

[a] *Department of Chemistry, University of Liverpool, United Kingdom, L69 7ZD.*
[b] *Institute of Materials Research and Engineering (IMRE), 2 Fusionopolis Way, Innovis, #08-03, Singapore 138634.*
[c] *Department of Chemistry, National University of Singapore, 3 Science Drive, Singapore 117543.*
* Corresponding authors: zhanghf@liv.ac.uk(HZ), x-li@imre.a-star.edu.sg (XL).
Electronic Supplementary Information (ESI) available: Additional SEM images, KOH soaking data, proposed pyrolysis mechanism, tables and additional references. See DOI: 10.1039/x0xx00000x

approach, seven N-containing groups were examined. It was found that pyridine group had the highest adsorption energy with CO_2 based on the Lewis acid-base interaction. However, pyridine group exhibited an even higher adsorption energy, which was attributed to the exceptional hydrogen-bonding between CO_2 and pyridine group.[23] Therefore, it is reasonable to suggest that only N-containing groups that exhibit strong basic sites and/or potential to form H bonding can improve CO_2 adsorption. With regards to H_2 storage, ultra-high surface areas and micropore volumes are considered to be the most important features for maximization of H_2 uptake, although a degree of heteroatom doping has also been suggested to improve uptake.[24,25] Monolithic structures can also hold certain advantages over ACs in powder and granular form, such as ease of handling and a relatively high volumetric adsorption.[11,26]

A common route to fabricating porous carbon monoliths is *via* so-called templating strategies, where a sacrificial templating entity is used to template the porous carbon structure.[15,27] The templates are generally either pre-formed porous structures (*hard-templating*), such as mesoporous silicas,[28-30] zeolites,[25,31] MOFs or colloidal crystals,[32] or self-assembled matrixes (*soft-templating*), such as polymer or surfactant networks.[33,34] Once the templated carbon has been prepared, the material can be subsequently activated in order to increase surface areas and micropore volumes.[35] Although templating methods can result in well-defined porous carbons with excellent gas sorption characteristics, certain disadvantages such as the complexity of the synthesis, assembly and subsequent removal of the templates (e.g., HF etching for silica templates), and a limited range of available precursors (typically low molecular weight, carbon-rich and cross-linkable precursors) limit their scope and economic viability.[15] Pre-formed and self-assembled porous structures, such as MOFs and conjugated microporous polymers (CMPs) may also be directly converted to high-surface area microporous carbons in some instances,[36-38] but high costs and complexity serve as a barrier to commercialization in these instances too.

Recently, ice crystals have been employed as simple, low-cost templating entities (*ice-templating*) to prepare templated porous carbons in a facile and cost-efficient manner.[39-41] Here, frozen solvent crystals act as the templates to direct the formation of a porous structure.[42,43] If suitable precursors are employed, the ice-templated structure can then be crosslinked and carbonized to form an ice-templated porous carbon (ITPC).[39-41] There are many kinds of templated carbons that have been prepared and evaluated for CO_2 and H_2 storage applications (Tables S1 & S2), however – to the best of our knowledge – this is the first report of an ice-templated carbon evaluated for this purpose.

The commercially available polymer PAN has previously been shown to be an attractive precursor for activated carbon for gas sorption applications. Nandi *et al.* recently reported a high CO_2 adsorption of 5.14 mmol g^{-1}, at ambient pressure and temperature, for a PAN-derived activated porous carbon.[44] Here, they firstly prepared a porous PAN monolith through their previously reported, template-free, thermally induced phase separation (TIPS) method,[45] followed by crosslinking, carbonizing and physical activation with CO_2. The high N content of the PAN polymer resulted in a high N-content activated carbon with excellent CO_2 sorption properties. Our group recently reported the preparation of ice-templated carbon monoliths from a PAN precursor.[39] In that study, PAN in dimethylsulfoxide solutions were directionally frozen and freeze dried to produce aligned ice-templated structures, which were then crosslinked and carbonized. The nitrogen rich carbon monoliths were evaluated as Li-ion battery anode materials where they displayed relatively good performance in comparison to other templated carbons.[39]

In this work, the ice-templating strategy with a convenient solvent-exchange process was employed to prepare porous PAN monoliths, instead of the energy-consuming freeze-drying procedure. After impregnating with KOH, the porous PAN monoliths were oxidatively crosslinked before carbonization & activation *via* pyrolysis (Fig. 1). The oxidative crosslinking is necessary to maintain the ice-templated structure upon pyrolysis, as it is for the manufacture of PAN-derived carbon fibres.[39,46] It was found that by varying the degree of KOH impregnation, the surface areas, porosity and level of N-doping of the materials could be varied allowing tuning of the material properties for specific applications, *i.e.*, CO_2 and H_2 adsorption (Table 1).

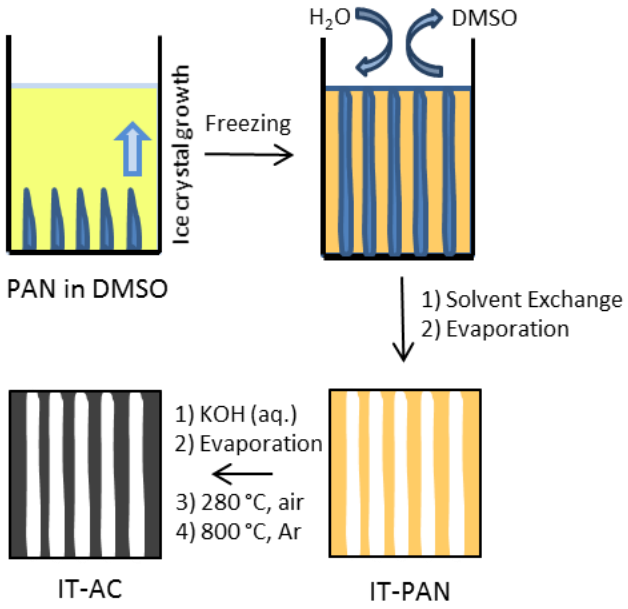

Fig. 1 Schematic representation of the process employed to prepare the IT-ACs.

2. Experimental

2.1. Materials

Polyacrylonitrile (PAN, M_w ~150,000), potassium hydroxide (> 85 %, pellets), sodium sulphate (> 99.0 %, anhydrous), dimethylsulfoxide (DMSO, > 99.9 %, anhydrous) and aqueous hydrochloric acid (37 %) were purchased from Sigma Aldrich

and used without further purification. Standard laboratory grade solvents and deionized water were used routinely.

2.2. Sample preparation

Preparation of ice-templated PAN monoliths

PAN (10 g) was dissolved in DMSO (100 ml) under stirring at 60 °C to form a 10 w/v % stock solution (based on the solvent volume). After cooling to room temperature, 6 x 4 ml portions of this stock solution were transferred to 12 ml disposable glass vials before being placed on the cooling element of a freezer (-18 °C) and left overnight. The frozen samples were then transferred into approximately 2 L of deionized water cooled to 0 °C with ice, and stirred to facilitate the solvent exchange between the frozen DMSO and liquid water. The samples were left in the 0 °C water for 2 h before the water and ice were refreshed. This process was repeated 4 times throughout the day, before the water-soaked samples were left to return to room temperature overnight. The water-soaked sampled were then soaked in acetone to displace the water and any residual DMSO. The samples were finally dried in a vacuum oven at 60 °C for 24 h. These samples are denoted IT-PAN10 (ice-templated PAN at 10 % concentration).

Incorporation of activating agent

KOH was dissolved in water to prepare 10 ml solutions at 5, 10, 20 and 50 w/v %. The prepared IT-PAN10 monoliths were separately soaked in these solutions for 2.5 h, under stirring and heating at 60 °C, before being removed and then dried in a vacuum oven at 60 °C for approximately 16 h. A blank sample soaked in deionized water (0 % KOH) was also prepared for comparison. These samples are denoted IT-PAN10-KOHX, where 'X' is the concentration of the KOH solution (in w/v %) that the monolith had been soaked in. To maximize the KOH uptake, one sample was soaked in 10 ml of 50 % KOH, which was left stirring at 60 °C for 36 h. Evaporation of water over this period concentrated the KOH to the point where it had begun precipitating out of solution. This sample is denoted IT-PAN10-KOHMAX, where 'MAX' represents the maximum attainable KOH soaking concentration.

Annealing and carbonization

The IT-PAN10-KOHX monoliths were subject to oxidative crosslinking by heating in a *Carbolite® Horizontal Compact Tube Furnace* to 280 °C in air (heating rate: 1 °C min^{-1}) for 1 h, and then allowed to cool naturally to room temperature. These annealed monoliths were then carbonized and activated by heating under a constant flow of argon (Ar flow rate: 100 ml min^{-1}) in the same furnace to 800 °C at a rate of 5 °C min^{-1}, holding 2.5 h at 800 °C, and cooling naturally to room temperature. The carbonized monoliths were then subject to a single acid wash (soaking in 2 M HCl for about 30 mins), before being washed thoroughly with water and ethanol to remove salts and other unwanted species formed upon carbonization. The carbonized and activated materials were then dried in a vacuum oven at 60 °C for approximately 16 h. These ice-templated, activated carbons materials are denoted IT-ACX, where 'X' is the concentration of the KOH solution (in w/v %) that the monolith had been soaked in.

Characterization

The samples were imaged and morphology determined using a JSM-6700F FE-SEM instrument with an accelerating voltage of 5 keV. Prior to imaging, samples were adhered to an aluminium stud using conductive copper tape, before being sputter-coated with a thin layer (~2 nm) of gold. Brunauer-Emmett-Teller (BET) specific surface areas and pore volumes were obtained *via* N_2 gas sorption at 77 K using a Micromeritics ASAP2420 volumetric adsorption analyser. The Barrett-Joyner-Halenda (BJH) pore size distributions were calculated from the same measurements. A pressure range of 0.06 – 0.3 P/P_0 was used for the BET surface area calculations and the reported pore volumes were given by the total single point adsorption of pores less than 170 nm radius at P/P_0 = 0.99. Samples were degassed at 200 °C under vacuum (10^{-5} bar) for 16 h before analysis. Powder X-ray diffraction (XRD) patterns were obtained with a Bunker GADDS XRD system with a Cu-α radiation source. Crystalline parameters of the carbons were calculated by employing the Bragg equation:

$$n\lambda = 2dsin\theta$$

And Scherrer equation:

$$\tau = \frac{K\lambda}{\beta cos\theta}$$

Where n is an integer, λ is the X-ray wavelength, d is the spacing between the atomic lattice planes, τ is the mean size of the crystalline domains, K is a dimensionless shape factor (taken as 0.9), β is the full width at half of the maximum (FWHM) intensity of the peaks, and θ is the angle of incidence between the incoming ray and the scattering planes. Raman spectra were recorded using a Renishaw InVia Raman Microscope fitted with a 633 nm laser, calibrated against a silicon wafer reference. X-ray photoelectron spectroscopy (XPS) measurements were taken with a VG ESCA LAB-220i XL XPS instrument with an exciting source of Al. Elemental analysis measurements were taken using a Flash EA 1112 Series CHNS-O Analyzer using cysteine sulfanilamide methionine as a standard and 8 x 5 mm

Table 1. BET surface area, total pore volume, and gas uptakes of porous carbon prepared by carbonization/activation of KOH-incorporated ice-templated PAN.

Sample	Mass KOH to PAN (wt. %)	BET surface area ($m^2 g^{-1}$)	Total Pore volume ($cm^3 g^{-1}$)	CO_2 adsorption 298K, 10 bar (mmol g^{-1})	H_2 adsorption 77K, 1.2 bar (wt. %)
IT-AC0	0	-	-	2.81	0.45
IT-AC5	7.21	9.8	0.007	3.43	0.844
IT-AC10	30.19	325.9	0.187	4.13	0.834
IT-AC20	62.07	792.2	0.432	7.71	No data
IT-AC50	90.09	1049.0	0.555	16.12	1.30
IT-ACMAX	365.88	2205.9	1.204	11.19	2.66

pressed Sn capsules to contain sample specimens. CO_2 and H_2 uptake measurements were collected using a Micromeritics ASAP2050 at 298 K and 77.3 K respectively. All samples were degassed at 120 °C for 15 h under vacuum (10^{-5} bar) prior to analysis.

3. Results and discussion

Fig. 1 depicts the process employed to prepare ice-templated and activated carbon monoliths (IT-ACs). Ice-templated PAN monoliths (IT-PAN10) were first prepared by freezing 10 w/v % solutions of PAN in DMSO at -18 °C by placing them in a cooling element of a freezer. Typically, solution samples are frozen in liquid nitrogen for ice templating, however the method demonstrated here requires only a freezer – and can therefore be regarded as a relatively simpler and greener route to prepare such materials. The fully frozen samples were then subject to solvent exchange (SE) by placing them in ice-cold (0 °C) water. To maintain the delicate structures after ice-templating, the frozen solvent crystal templates need to be removed without melting. In the case of ice crystals melting, the liquid solvent could re-dissolve the templated structure resulting in loss of the ice-templated morphology. Typically, freeze-drying is employed to achieve this, *i.e.,* by direct sublimation of the solvent crystals under vacuum. However, freeze-drying is a relatively energy intensive process and is not suitable for most solvents other than water. Although we have previously demonstrated the removal of DMSO from ice-templated PAN via freeze-drying,[39] the SE method described here represents a simpler, greener and faster process for its removal. Since the melting point of DMSO is 19 °C and miscible with water, by performing the SE at 0 °C it ensures the slow dissolution of frozen DMSO into water whilst the remaining DMSO is still frozen until fully dissolved. Also, because PAN is hydrophobic and insoluble in water, by regularly refreshing the water and ice several times, it ensures the removal of the DMSO through dilution without damaging the ice-templated structure. Removal of the water (and any residual DMSO) is then achieved by SE with acetone at room temperature, which can then be removed easily by placing in a fume cupboard and vacuum drying. SEM images confirmed the presence of an ice-templated morphology, indicating that the SE had worked successfully (Fig. S1).

The dried IT-PAN10 monoliths were then soaked in aqueous KOH solutions at various concentrations (5, 10, 20 and 50 w/v %) at 60 °C for 2.5 h, before being removed from the solution and dried in a vacuum oven for approximately 16 h. To maximize KOH uptake, one sample was soaked in 50 % KOH at 60 °C for 36 h with the aqueous solution exposed to air; the evaporation of water over this period increased the KOH concentration, leading to the precipitation of KOH out of solution and crystalized on the surface and within the pores of the ice-templated PAN monolith. Due to the very low concentration of CO_2 (~ 0.04 %) in atmosphere, the effect of K_2CO_3 formed by reaction of CO_2 and KOH is minimal. The limited mass transport for any formed K_2CO_3 may further minimize its effect.

The masses of the samples before and after soaking are presented in Table 1 and Fig. S2, where it can be seen that a higher KOH soaking concentration resulted in a greater uptake of KOH, as would be expected. It was observed that, upon soaking the samples in KOH, the monoliths changed from their original white coloration to an orange/red colour (Fig. S3). This was attributed to a base-catalysed intra-molecular cyclization of the nitrile backbone of the PAN polymer leading to a conjugated ladder-type polymer backbone (Fig. S4).[47] This mechanism was likely catalysed by trace of DSMO within the polymer; as it was recently shown that DMSO in the presence of alkali metal hydroxides could form superbasic dimethyl sulfoxy anions that could nucleophilically attack nitrile groups at room temperature.[48] The darkening of the polymer over time was attributed to an increasing extent of conjugation lowering the band gap between HOMO and LUMO molecular orbitals.[49]

After KOH infusion and drying, the monoliths were subjected to oxidative annealing by heating in a tube furnace to 280 °C in air. This process induces cyclization and crosslinking of the PAN polymers, increasing their stability and allowing them to retain their morphology and a high yield on carbonization.[46] The crosslinked precursors were then carbonized by heating to

800 °C under an argon atmosphere, followed by washing with 2 M HCl and water, and drying in a vacuum oven.

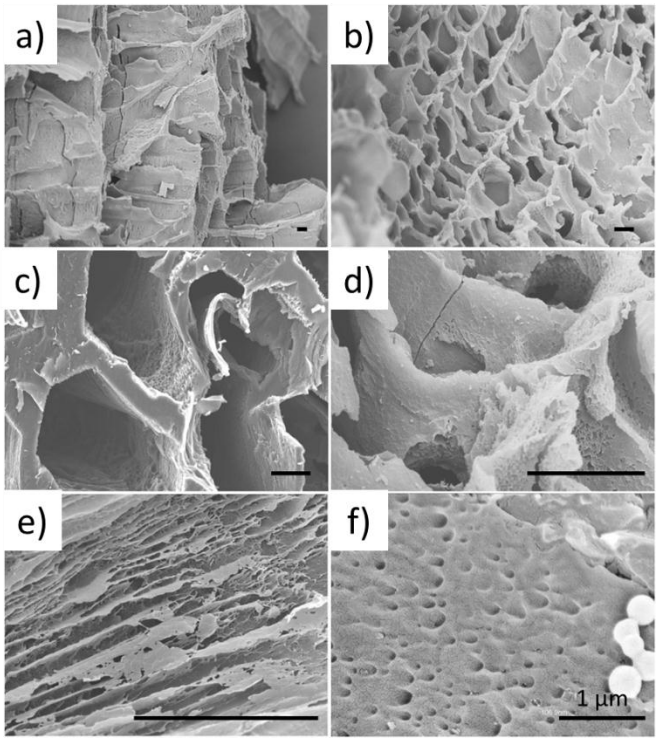

Fig. 2 SEM images of IT-AC20 at various magnifications: a) x300, b) x700, c) x1400, d) x3700 e) x6500 f) x30000 magnifications. Scale bar = 10 µm unless otherwise indicated.

After carbonization, the monoliths were imaged *via* FESEM, which confirmed the retention of the ice-templated morphology (Fig. S5). As a representative example, IT-AC20 was imaged in detail, displaying aligned, ice-templated macropores with a broad size distribution, spanning 100 nm to over 100 µm (Fig. 2). Freezing in liquid nitrogen would have produced smaller and more unimodal pores,[50] however freezing at -18 °C in a freezer was employed for these experiments to demonstrate the green credentials of this process.

N_2 gas sorption measurements were performed on the samples to examine how the porosity and surface area varied with KOH uptake (Fig. 3). The measurement failed for the non-activated, control sample (IT-AC0) – likely due to the surface area being too low for an accurate measurement. The measurement was successful for the other samples, which had isotherms that can be categorized as type I according to IUPAC nomenclature,[51] indicating a predominantly microporous structure (Fig. 3a). Samples IT-AC50 and IT-ACMAX also displayed small hysteresis loops at high partial pressures, indicating the presence of mesopores in addition to micropores. Analysis of the isotherms showed that the BET surface area increased with increasing KOH uptake, suggesting a greater degree of activation with higher KOH content (Table 1, Fig. S6). With the highest KOH content, IT-ACMAX had the highest BET surface area of 2206 $m^2\ g^{-1}$ – a value within the normal range for chemically activated carbons (typically between 500 and 3000 $m^2\ g^{-1}$).[11] The yields of the activated carbon are in the range of 13.8 – 57.8 %, varying by the amount of KOH incorporated (IT-ACMAX, 13.8 %; IT-AC50, 24.7 %; IT-AC20, 33.0 %; IT-AC10, 49.2 %; IT-AC5, 54.6 %; IT-AC0, 57.8 %). Pore size analysis of the isotherms showed the majority of pores for the highly activated samples being in the micropore (< 2 nm) domain, with a clear trend of an increasing micropore volume with increasing KOH content (Fig. 3b). This analysis also revealed the presence of mesoporous, mainly between the size range of 10 – 30 nm, and macropores (which may be further corroborated by Hg intrusion porosimetry), confirming a hierarchical micro-, meso- and macro-pore structure.

XRD and Raman measurements were taken to study the nanostructure and crystallinity of the carbons (Fig. 4). XRD revealed two broad Bragg reflections at approximately 25 and 44°, which were attributed to the (002) and (101) reflections

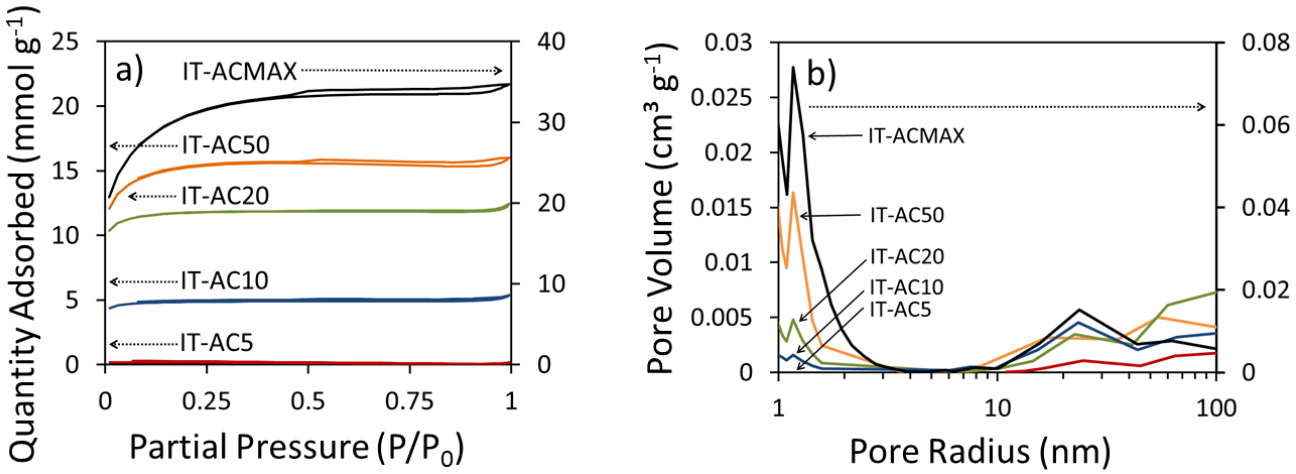

Fig. 3 Nitrogen sorption data for the IT-ACs: a) isotherms, b) pore size distribution charts.

Table 2 Summary of XRD and Raman data for the IT-ACs

Sample	L_c (Å)	L_a (Å)	d_{002} (Å)	Sheets per crystallite	I_D/I_G
IT-AC0	21.15	29.90	3.562	5.96	1.128
IT-AC5	24.46	35.22	3.494	7.00	1.220
IT-AC10	23.94	33.94	3.527	6.79	1.234
IT-AC20	22.64	35.44	3.530	6.41	1.095
IT-AC50	23.30	46.30	3.465	6.72	1.142
IT-ACMAX	19.71	26.99	3.410	5.78	1.012

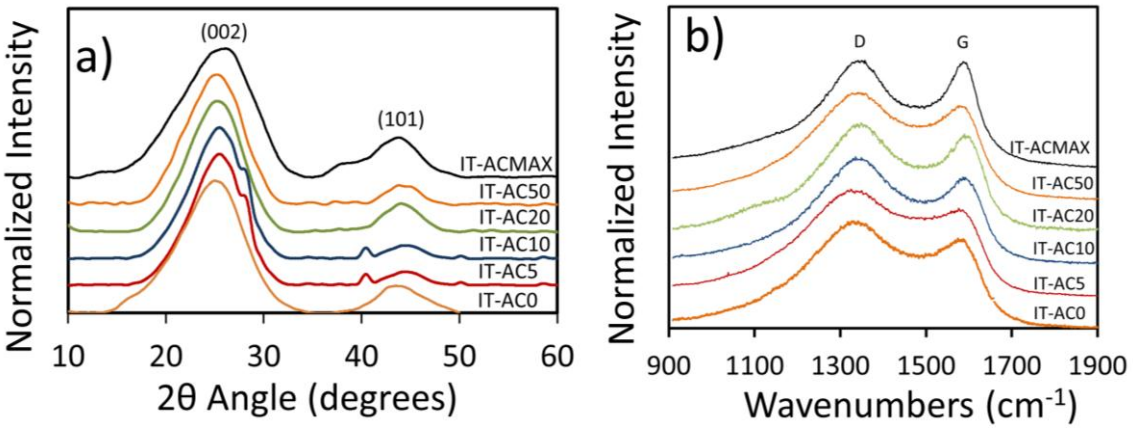

Fig. 4 a) XRD and b) Raman data for the IT-AC samples

typically observed for microcrystalline, semi-graphitic carbons. The average size parameters of the microcrystallites (L_c and L_a) were calculated by employing the Scherrer equation, and the average interlayer spacing of adjacent graphite sheets was calculated by employing the Bragg equation (Table 2). The data does not show a large difference between samples, indicating that the degree of KOH activation does not significantly affect the crystallinity of the carbon samples, despite the introduction of micropores. First order Raman spectroscopy revealed two peaks at approximately 1340 and 1590 cm^{-1}, the former corresponding to the A_{1g} mode associated with defect in the carbon structure (D-band) and the latter corresponding to the E_{2g} mode of graphitic carbon (G-band).[52] The ratio of the intensity of the D- and G- bands (I_D/I_G) for the carbons was calculated and is presented in Table 2. As with XRD, no clear trend between KOH uptake and these parameters were observed.

Elemental (CHN) analysis and XPS spectroscopy were employed to investigate the elemental content of the samples (Table 3). The results of the CHN analysis show a very high N content (15 – 17 wt. %) for all samples other than IT-ACMAX, which had a much lower N content of 1.29 wt. %. This decrease in N content could be attributed to the oxidative nature of the KOH activation agent, which – at high concentrations – preferentially reacts with the relatively less stable C-N bonds over C-C bonds, resulting in a lower N content. The same trend was also observed with XPS, which detected 10 – 15 At. % N for all samples other than IT-ACMAX – for which it detected zero (Fig. 5, Table 3). Due to the quantitative nature of the CHN analysis measurement, it was taken as the more reliable measurement for bulk N content within the samples — as XPS only provides a superficial quantification of the measured material. The N1s spectrum of the XPS was analysed in order to ascertain the chemical environment of the N within the IT-ACs (Fig. 5, inset). Each sample, other than IT-ACMAX, could be fitted into two component peaks at approximately 398 and 401 eV, corresponding to pyridinic and quaternary nitrogen, respectively. The relative ratios of the peaks are reported in Table 3, which shows an increase in quaternary groups relative to pyridinic groups as KOH uptake increases from IT-AC0 to IT-AC10 & then decrease to IC-AC50, and a notable increasing percentage of pyridinic N for IT-AC 10, IT-AC 20 & IT-AC 50.

A CO_2 uptake study of the IT-ACs was performed at 298 °C and 10 bar pressure, the results of which are presented in Fig. 6a & 6b and Table 1. It can be seen that as the soaking concentration of KOH increases, the CO_2 uptake also increases in a roughly linear fashion, up to a maximum of 16.12 mmol g^{-1} for sample IT-AC50 (Fig. 6b). However, the sample with the

Table 3 Element Compositions of the carbon materials by elemental analysis and XPS analysis

Sample	Elemental Analysis			XPS Analysis				
	C (wt. %)	H (wt. %)	N (wt. %)	C (wt. %)	N (wt. %)	O (wt. %)	Pyridinic N (At. %)	Quaternary N (At. %)
IT-AC0	65.1	1.93	16.1	76.91	12.13	10.96	63.2	36.8
IT-AC5	71.4	0.70	17.5	81.79	12.36	5.85	41.8	58.2
IT-AC10	72.4	1.46	17.2	80.68	14.59	4.73	37.6	62.4
IT-AC20	73.4	2.03	14.8	82.91	11.34	5.76	37.9	62.1
IT-AC50	71.9	1.77	14.9	87.29	10.34	2.38	43.1	56.9
IT-ACMAX	84.9	2.01	1.29	95.06	0	4.94	0	0

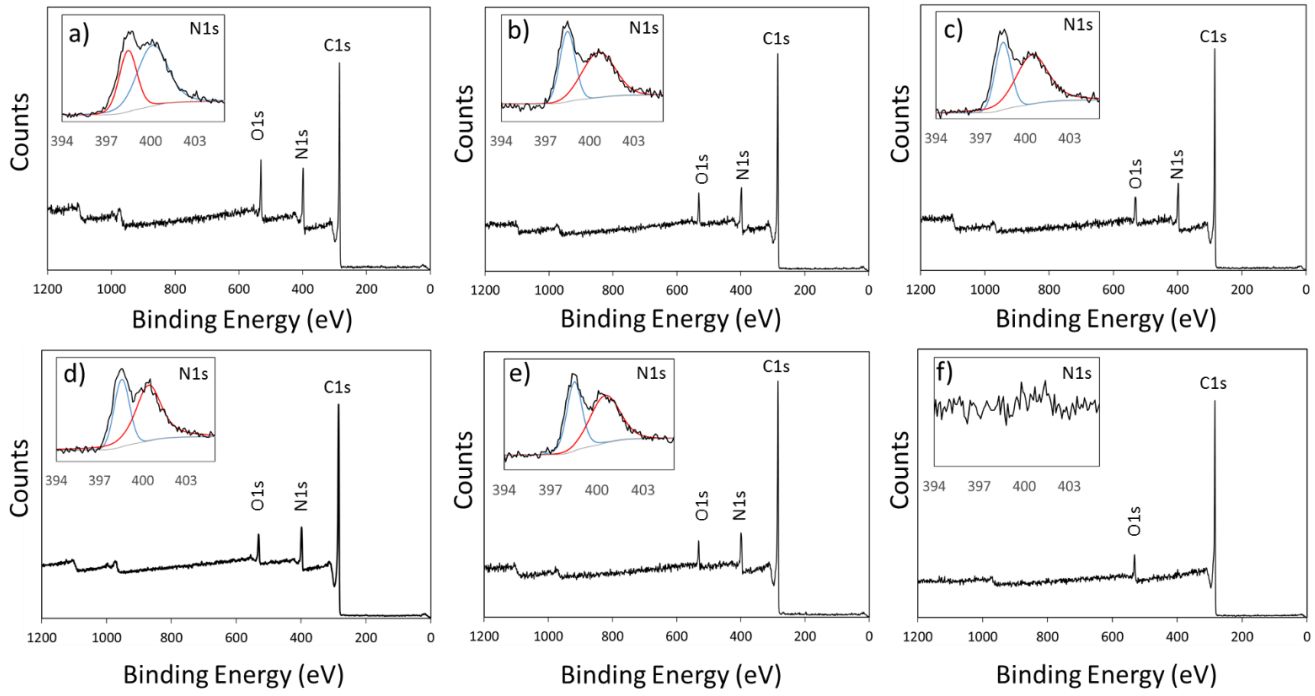

Fig. 5 XPS data for a) IT-AC0, b) IT-AC5, c) IT-AC10, d) IT-AC20, e) IT-AC50 and f) IT-ACMAX, with N1s scans inset.

highest KOH loading (IT-ACMAX), the CO_2 uptake drops to 11.19 mmol g^{-1}. This trend may be explained by the change in surface areas and N content as the KOH loading increases. For samples IT-AC5, IT-AC10, IT-AC20 and IT-AC50, the increased KOH loading increases the surface area whist only having a minor effect on the N content. The increasing surface area provides a greater area for the physisorption of CO_2 molecules and thus the CO_2 adsorption is increased. However, for the IT-ACMAX sample, although the surface area is over twice as high as the IT-AC50 sample, the N content is significantly lower (1.29 wt. %, vs. 14.9 wt. %). It has been well documented, both experimentally and by modelling, that doping of N into carbon materials could create surface basic sites and enhance adsorption of CO2.[17-23,53] The combination of high surface area and high N content in the sample IT-AC50 has resulted in the highest CO_2 uptake among the samples tested. The higher percentage of pyridinic N in IT-AC50 (comparing the last 4 samples in Table 3), which was shown to give high CO_2 adsorption energy,[23] contribute favourably to the enhanced CO_2 uptake. The shapes of the CO_2 sorption isotherms also suggest a different mechanisms occurring between the samples: whilst the IT-AC50 sample has a very reversible adsorption-desorption cycle, IT-ACMAX has significant hysteresis suggesting delayed release of CO_2 after the pressure drops, which could result from the higher percentage of micropores and convoluted pore structures.[17] The adsorption of 16.12 mmol g^{-1} for the IT-AC50

Table 4 Comparison with the CO_2 uptakes from porous materials reported in literature under similar test conditions.

Materials	BET Surface area (m^2 g^{-1})	N content (wt. %)	CO_2 Adsorption (mmol g^{-1})	Test Conditions	Ref.
Direct carbonization of MOF-5	2734	NA	12.5	300 K, 10 bar	16
Active carbon from mesoporous silica template	1181	13	10.5	298 K, 8 bar	54
Freeze drying, carbonization & activation of polyaniline gel	4196	0.55	14.5	298 K, 10 bar	55
MOF-205	4460	0	10.9	298 K, 10 bar	56
COF-102	3620	0	15.5	298 K, 10 bar	8
Porous polymer network (PPN)-4	6461	0	11.6	295 K, 10 bar	57
Hyperporous carbons from hypercrosslinked polymer Py800	4334	1.42	22.0	298 K, 10 bar	58
Hydrothermal carbonization of biomass & KOH activation	3144	NA	15.5	298 K, 10 bar	59
KOH activation of air-carbonized wood	2315	NA	16.1	298 K, 10 bar	60
Biochar & KOH activation	3167	NA	15.0	298 K, 10 bar	61
Hydrothermal carbonization of sucrose & KOH activation	2431	NA	12.3	298 K, 10 bar	62
Porous carbon by ice templating & KOH activation	1049	14.9	16.1	298 K, 10 bar	This Work

sample at 298 K and 10 bar is among the highest in comparison to porous carbons and other materials such as metal-organic frameworks (MOFs), covalent organic frameworks (COFs) and porous polymer tested under similar conditions in literature (Table 4). In spite of the high performance in CO_2 adsorption from our carbon IT-AC50, the surface area is very low compared to other carbon materials and MOFs/COFs (Table 4). This suggest the importance of N-doping in carbon materials for CO_2 adsorption. A more detailed comparison of our carbon materials with other templated porous carbons under different test pressures is also given in Table S1, demonstrating very good CO_2 uptake of the IT-AC50 from this current work. Furthermore, the highly reversible sorption characteristics of the IT-AC50 as indicated by the shape of the isotherm may allow facile regeneration of the materials. There is scope for even higher adsorption at further increased pressures as the isotherm for IT-AC50 has yet to plateau even at 10 bar.

A H_2 uptake study of the IT-ACs was also performed, at 77 K and 1.2 bar pressure (Fig. 6c & 6d, Table 3). This showed a roughly linear increase between KOH uptake and H_2 adsorption, with a maximum of 2.66 wt. % H_2 adsorption for the IT-ACMAX sample (Fig. 6d). Unlike the CO_2 uptake study, H_2 adsorption was much less dependent on the N content of the sample – but instead had a fairly linear relationship with surface area since the surface areas are approximately in linear relationship with the KOH uptake in porous PAN (Fig. S6). This is in concordance with other reports which also conclude that surface area is the most important property for maximizing H_2 adsorption.[11] The performance of our carbon materials for H_2 uptake is quite good and particularly when compared to other porous carbons, as shown in Table S2.

4. Conclusions

In conclusion, we have demonstrated a facile and relatively green method for the preparation of hierarchically porous templated carbons *via* an ice-templating and chemical activation process. The degree of activation, and hence surface area and N content, could be varied by simply changing the concentration of the soaking KOH solution, to be suitable for different gas uptake applications. The material with the highest degree of activation (IT-ACMAX) had a surface area of 2205 m^2 g^{-1}, an N content of 1.29 wt. % and had the highest H_2 adsorption of 2.66 wt. % at 77 K and 1.2 bar. The material with the highest CO_2 adsorption (IT-AC50) had both a high surface area (1049 m^2 g^{-1}) and N content (14.9 wt. %) – with a maximum CO_2 adsorption of 16.12 mmol g^{-1} at 298 K and 10 bar of pressure. The high CO_2 uptake is particularly interesting because higher surface area is usually required to achieve such high uptake thus suggesting the fundamental role of surface chemistry, namely high nitrogen content. Further studies are required to understand the exact adsorption mechanism of CO_2

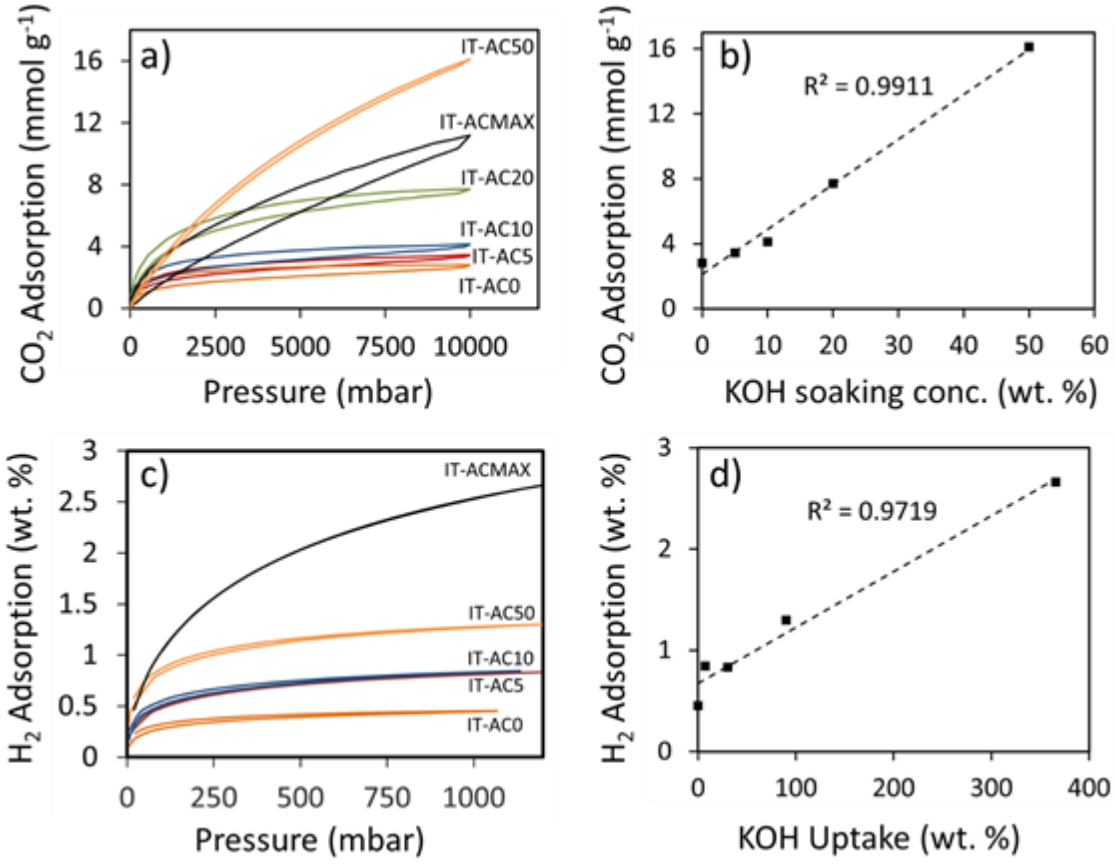

Fig. 6 a) CO_2 adsorption isotherm, b) relationship between CO_2 adsorption and KOH soaking concentration, c) H_2 adsorption isotherms and d) relationship between H_2 adsorption and KOH uptake in porous polymer.

in these carbon materials. This performance is in league with the highest CO_2 uptakes from carbon and other porous materials and also very good for H_2 uptake, in spite of the facile and scalable material preparation process.

Acknowledgements

ADR is grateful for the joint PhD studentship between the University of Liverpool and the A*Star Research Attachment Program (ARAP) in Singapore. We acknowledge the Centre of Materials Discovery in the University of Liverpool for access to their state of the art facilities and the help from Mr Rob Clowes.

References

1 R. S. Haszeldine, *Science,* 2009, **325**, 1647.
2 D. M. D'Alessandro, B. Smit and J. R. Long, *Angew. Chem. Int. Ed.,* 2010, **49**, 6058.
3 J. Gibbins and H. Chalmers, *Energy Policy,* 2008, **36**, 4317.
4 B. Metz, *Climate Change 2001: Mitigation: Contribution of Working Group III to the Third Assessment Report of the Intergovernmental Panel on Climate Change*, Cambridge University Press, **2001**.
5 P. Jena, *J. Phys. Chem. Lett.,* 2011, **2**, 206.
6 L. J. Murray, M. Dincă and J. R. Long, *Chem. Soc. Rev.,* 2009, **38**, 1294.
7 K. Sumida, D. L. Rogow, J. A. Mason, T. M. McDonald, E. D. Bloch, Z. R. Herm, T.-H. Bae and J. R. Long, *Chem. Rev.,* 2012, **112**, 724.
8 H. Furukawa and O. M. Yaghi, *J. Am. Chem. Soc.,* 2009, **131**, 8875.
9 R. Chatti, A. K. Bansiwal, J. A. Thote, V. Kumar, P. Jadhav, S. K. Lokhande, R. B. Biniwale, N. K. Labhsetwar and S. S. Rayalu, *Micropor. Mesopor. Mater.,* 2009, **121**, 84.
10 R. T. Woodward, L. A. Stevens, R. Dawson, M. Vijayaraghavan, T. Hasell, I. P. Silverwood, A. V Ewing, T. Ratvijitvech, J. D. Exley, S. Y. Chong, F. Blanc, D. J. Adams, S. G. Kazarian, C. E. Snape, T. C. Drage and A. I. Cooper, *J. Am. Chem. Soc.,* 2014, **136**, 9028.
11 M. Sevilla and R. Mokaya, *Energy Environ. Sci.,* 2014, **7,** 1250.
12 M. G. Plaza, S. García, F. Rubiera, J. J. Pis and C. Pevida, *Chem. Eng. J.,* 2010, **163**, 41.
13 M. Radosz, X. Hu, K. Krutkramelis and Y. Shen, *Ind. Eng.*

Chem. Res., 2008, **47**, 3783.
14 T. L. P. Dantas, S. M. Amorim, F. M. T. Luna, I. J. Silva, D. C. S. de Azevedo, A. E. Rodrigues and R. F. P. M. Moreira, *Sep. Sci. Technol.,* 2009, **45**, 73.
15 A. D. Roberts, X. Li and H. Zhang, *Chem. Soc. Rev.* 2014, **43**, 4341.
16 G. Srinivas, V. Krungleviciute, Z.-X. Guo and T. Yildirim, *Energy Environ. Sci.,* 2014, **7**, 335.
17 G.-P. Hao, W.-C. Li, D. Qian and A.-H. Lu, *Adv. Mater.,* 2010, **22**, 853.
18 G. Puxty, R. Rowland, A. Allport, Q. Yang, M. Brown, R. Burns, M. Maeder and M. Attalla, *Environ. Sci. Technol.,* 2009, **43**, 6427.
19 M. Sevilla, P. Valle-Vigón and A. B. Fuertes, *Adv. Funct. Mater.,* 2011, **21**, 2781.
20 J. Wei, D. Zhou, Z. Sun, Y. Deng, Y. Xia and D. Zhao, *Adv. Funct. Mater.,* 2013, **23**, 2322.
21 L. Wang and R. T. Yang, *J. Phys. Chem. C,* 2012, **116**, 1099.
22 W. Xing, C. Liu, Z. Zhou, L. Zhang, J. Zhou, S. Zhuo, Z. Yan, H. Gao, G. Wang and S.Z. Qiao, *Energy Environ. Sci.,* 2012, **5**, 7323.
23 G. Lim, K. B. Lee and H. C. Ham, *J. Phys. Chem. C.,* 2016, **120**, 8087.
24 Z. Zhou, X. Gao, J. Yan and D. Song, *Carbon,* 2006, **44**, 939.
25 Z. Yang, Y. Xia, X. Sun and R. Mokaya, *J. Phys. Chem. B,* 2006, **110**, 18424.
26 G.-P. Hao, W.-C. Li, D. Qian, G.-H. Wang, W.-P. Zhang, T. Zhang, A.-Q. Wang, F. Schüth, H.-J. Bongard and A.-H. Lu, *J. Am. Chem. Soc.,* 2011, **133**, 11378.
27 H. Nishihara and T. Kyotani, *Adv. Mater.,* 2012, **24**, 4473.
28 C. Vix-Guterl, E. Frackowiak, K. Jurewicz, M. Friebe, J. Parmentier and F. Béguin, *Carbon,* 2005, **43**, 1293.
29 M. Kruk, B. Dufour, E. B. Celer, T. Kowalewski, M. Jaroniec and K. Matyjaszewski, *J. Phys. Chem. B,* 2005, **109**, 9216.
30 M. Sevilla and A. B. Fuertes, *J. Colloid Interface Sci.,* 2012, **366**, 147.
31 N. P. Stadie, J. J. Vajo, R. W. Cumberland, A. A. Wilson, C. C. Ahn and B. Fultz, *Langmuir,* 2012, **28**, 10057.
32 S.-W. Woo, K. Dokko, H. Nakano and K. Kanamura, *J. Mater. Chem.,* 2008, **18**, 1674.
33 E. Ramasamy, J. Chun and J. Lee, *Carbon,* 2010, **48**, 4563.
34 Y. Hu, H. Liu, Q. Ke and J. Wang, *J. Mater. Chem. A,* 2014, **2**, 11753.
35 M. Sevilla, N. Alam and R. Mokaya, *J. Phys. Chem. C,* 2010, **114**, 11314.
36 H.-L. Jiang, B. Liu, Y.-Q. Lan, K. Kuratani, T. Akita, H. Shioyama, F. Zong and Q. Xu, *J. Am. Chem. Soc.,* 2011, **133**, 11854.
37 J.-S. M. Lee, T.-H. Wu, B. M. Alston, M. E. Briggs, T. Hasell, C.-C. Hu and A. I. Cooper, *J. Mater. Chem. A,* 2016, **4**, 7665.
38 W. Chaikittisilp, K. Ariga and Y. Yamauchi, *J. Mater. Chem. A,* 2013, **1**, 14.
39 A. Roberts, S. Wang, X. Li and H. Zhang, *J. Mater. Chem. A,* 2014, **2**, 17787.
40 A. D. Roberts, X. Li and H. Zhang, *Carbon,* 2015, **95**, 268.
41 H. Nishihara, S. R. Mukai and H. Tamon, *Carbon,* 2004, **42**, 899.
42 L. Qian and H. Zhang, *J. Chem. Technol. Biotechnol.*, 2011, **86**, 172.
43 M. C. Gutiérrez, M. L. Ferrer and F. del Monte, *Chem. Mater.,* 2008, **20**, 634.
44 M. Nandi, K. Okada, A. Dutta, A. Bhaumik, J. Maruyama, D. Derks and H. Uyama, *Chem. Commun.,* 2012, **48**, 10283.
45 K. Okada, M. Nandi, J. Maruyama, T. Oka, T. Tsujimoto, K. Kondoh and H. Uyama, *Chem. Commun.,* 2011, **47**, 7422.
46 M. S. A. Rahaman, A. F. Ismail and A. Mustafa, *Polym. Degrad. Stab.,* 2007, **92**, 1421.
47 O. Şanli, *Eur. Polym. J.,* 1990, **26**, 9.
48 H. Chen, W. Dai, Y. Chen, Q. Xu, J. Chen, L. Yu, Y. Zhao, M. Ye and Y. Pan, *Green Chem.,* 2014, **16**, 2136.
49 P. Atkins, J. de Paula, *Elements of Physical Chemistry*, OUP Oxford, **2013**.
50 H. Zhang, I. Hussain, M. Brust, M. F. Butler, S. P. Rannard and A. I. Cooper, *Nat. Mater.,* 2005, **4**, 787.
51 M. Thommes, K. Kaneko, A.V. Neimark, J.P. Olivier, F. Rodriguez-Reinoso, J. Rouquerol, and K.S.W. Sing, *Pure Appl. Chem.*, 2015, **87**, 1051.
52 Y. Wang, D. C. Alsmeyer and R. L. McCreery, *Chem. Mater.,* 1990, **2**, 557.
53 R. Babarao, S. Dai and D. Jiang, *J. Phys. Chem. C.,* 2012, **116**, 7106.
54 Y. Zhao, L. Zhao, K. X. Yao, Y. Yang, Q. Zhang, and Y. Han, *J. Mater. Chem.*, 2012, **22**, 19726.
55 J. He, J. W. F. To, P. C. Psarras, H. Yan, T. Atkinson, R. T. Holmes, D. Nordlund, Z. Bao, and J. Wilcox, *Adv. Energy Mater.*, 2016, **6**, 1502491.
56 H. Furukawa, N. Ko, Y.B. Go, N. Aratani, S. B. Choi, E. Choi, A. Ö. Yazaydin, R. Q. Snurr, M. O'Keeffe, J. Kim and O. M. Yaghi, *Science*, 2010, **329**, 424.
57 D. Yuan, W. Lu, D. Zhao and H.-C. Zhou, *Adv. Mater.* 2011, **23**, 3723.
58 J.-S. M. Lee, M. E. Briggs, T. Hasell and A. I. Cooper, *Adv. Mater.* 2016, **28**, 9804.
59 H. M. Coromina, D.A. Walsh and R. Mokaya, *J. Mater. Chem. A*, 2016, **4**, 280.
60 E. Haffner-Staton, N. Balahmar and R. Mokaya, *J. Mater. Chem. A*, 2016, **4**, 13324.
61 Y. Li, G. Ruan, A.S. Jalilov, Y.R. Tarkunde, H. Fei and J. M. Tour, *Carbon*, 2016, **107**, 344.
62 A.S. Mestre, C. Freire, J. Pires, A.P. Carvalho and M. L. Pinto, *J. Mater. Chem. A*, 2014, **2**, 15337.

Electronic Supplementary Information

Nitrogen-rich activated carbon monoliths via ice-templating with high CO_2 and H_2 adsorption capacities

Aled D. Roberts,[a,b] Jet-Sing M. Lee,[a] Siew Yee Wong,[b] Xu Li*[b,c] and Haifei Zhang*[a]

[a] *Department of Chemistry, University of Liverpool, United Kingdom, L69 7ZD.*
[b] *Institute of Materials Research and Engineering (IMRE), 2 Fusionopolis Way, Innovis, #08-03, Singapore 138634.*
[c] *Department of Chemistry, National University of Singapore, 3 Science Drive, Singapore 117543.*
E-mail: zhanghf@liv.ac.uk(HZ), x-li@imre.a-star.edu.sg (XL).

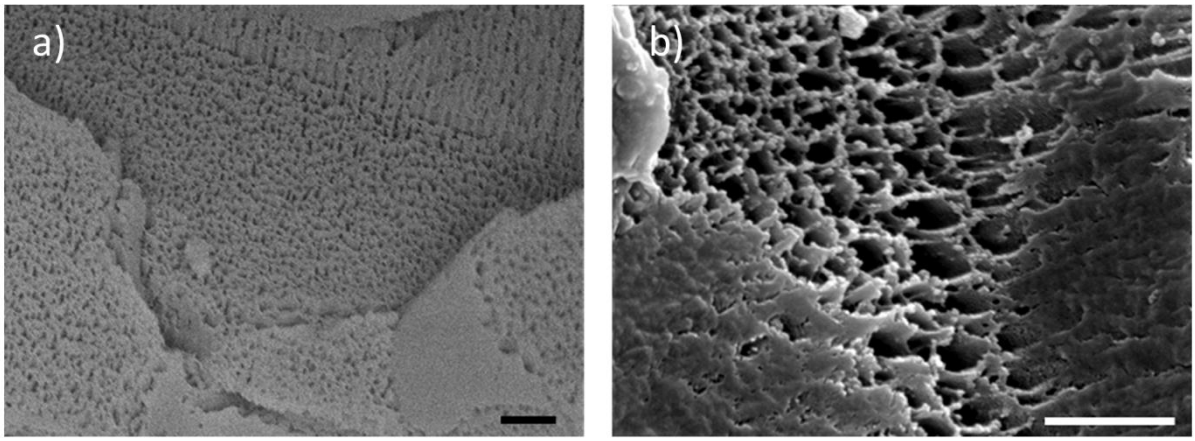

Fig. S1 SEM images of the ice-templated PAN polymer (IT-PAN10) at a) x11000 and b) x27000 magnification. Scale bar = 1 µm

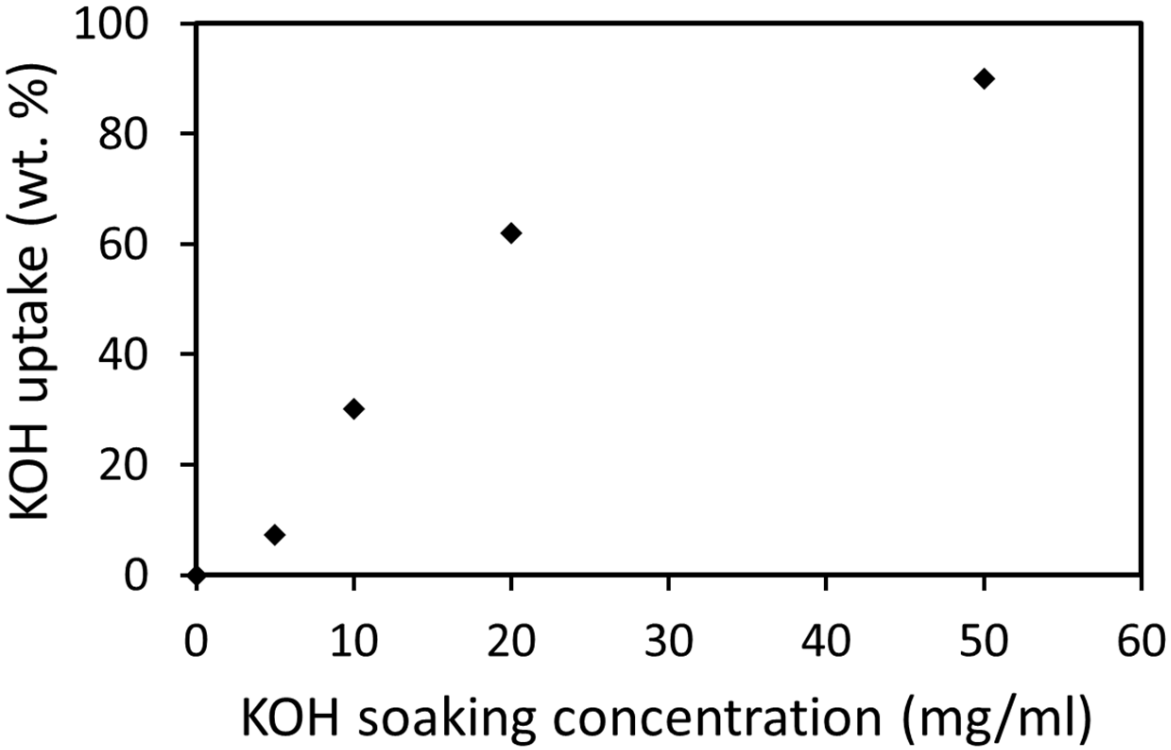

Fig. S2 Relationship between KOH soaking concentration and KOH uptake within the ice-templated porous PAN.

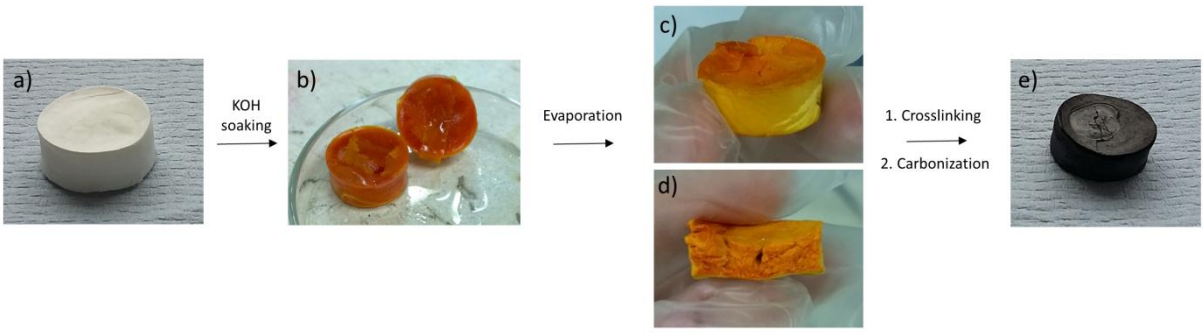

Fig. S3 a) IT-PAN10 monolith, b) after soaking in 10 mg ml^{-1} aqueous KOH, c) after KOH soaking and drying, d) cross-sectional view after KOH soaking and drying e) after crosslinking and carbonization (IT-AC10).

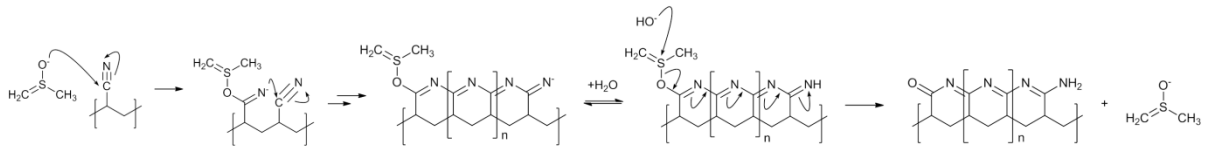

Fig. S4 Proposed base-catalysed intra-molecular cyclization of the nitrile backbone of the PAN polymer into a conjugated ladder-type polymer

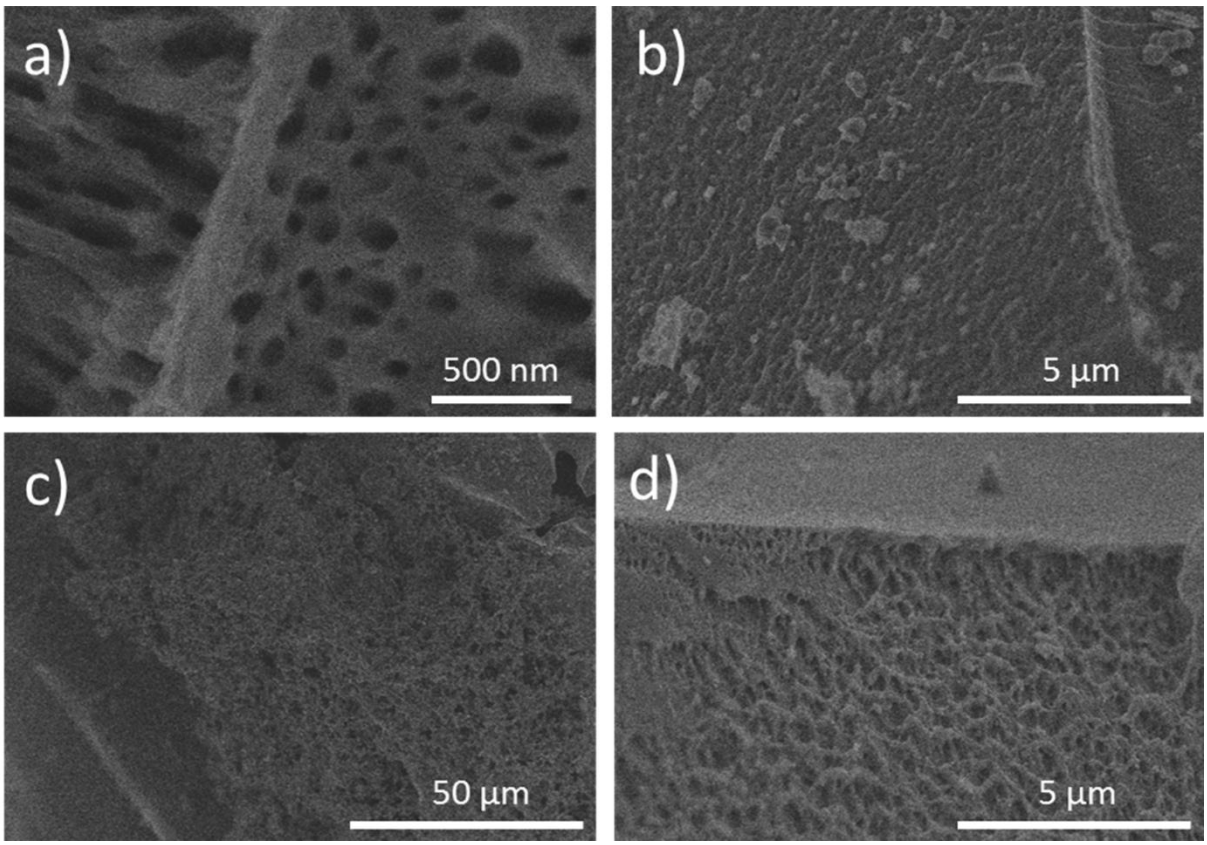

Fig. S5 SEM images of carbonized samples of ice-templated PAN: a) IT-AC5, b) IT-AC10, c) IT-AC50 and d) IT-ACMAX

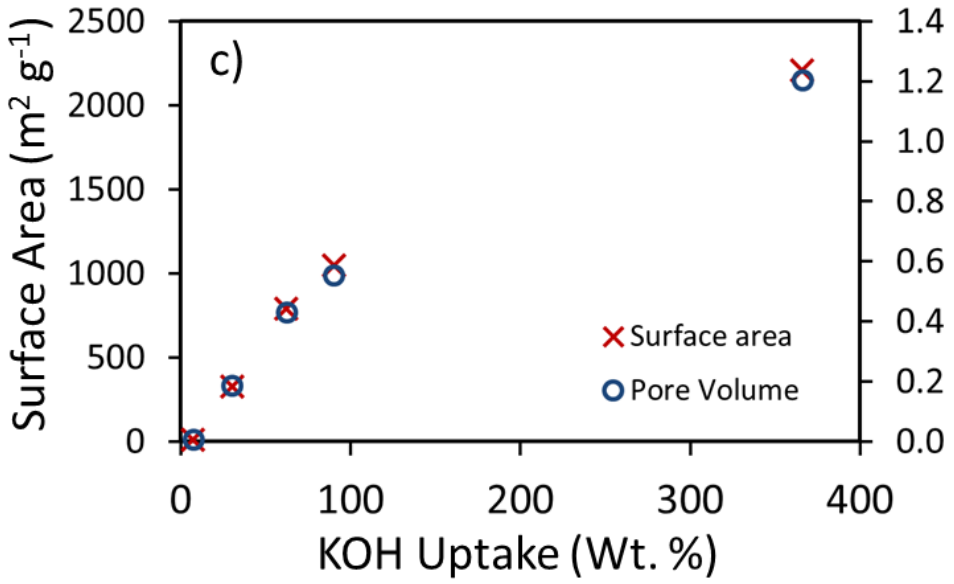

Fig. S6. The relationship of the BET surface areas for the porous activated carbon with the KOH uptake into the porous ice-templated PANs.

Table S1 CO_2 adsorption capacities of various templated carbons published in the literature

Template	Precursor	Method	BET SSA ($m^2 g^{-1}$)	N-content (wt. %)	CO_2 Adsorption (mmol g^{-1})	Conditions	Ref.
Pluronic F127	Resorcinol & Formaldehyde (RF)	RF polymerization with amine, carbonization	670	0.28	3.3	298 K, ~1 Bar	[1]
Pluronic F127	Resorcinol & Formaldehyde (RF)	RF polymerization with amine, carbonization and KOH activation	1613	0.68	3.1	298 K. 0.95 Bar	[2]
Pluronic F127	Dicyandiamide, Resol	Polymerization, carbonization	1417	6.7	3.2	298 K, 1 Bar	[3]
Pluronic 123	Polypyrrole	Polymerization of pyrrole, carbonization	941	5.8	4.5	298 K, 1 Bar	[4]
Benzimidazole-Linked Polymers	Benzimidazole-Linked Polymers	Direct carbonization (polymer acts as precursor and template) & KOH activation	1630	7.9	5.8	298 K, 1 Bar	[5]
Hypercrosslinked porous polymer (COP)	Hypercrosslinked porous polymer (COP)	Direct carbonization & KOH activation	1950	Not given	7.6	273 K, 1 Bar	[6]
Zeolite EMC-2	Acetonitrile	CVD	2559	6 - 7	4.0	298 K, ~1Bar	[7]
Zeolite EMC-2	Acetonitrile	CVD	3360	4.7	4.4	298 K, 1 Bar	[8]
ZIF-69	ZIF-69	Direct carbonization (ZIF acts as template and precursor) & KOH activation	2264	1.2	4.8	273 K, 1 Bar	[9]
MOF-5	MOF-5	Direct carbonization (MOF acts as template and precursor)	2734	Not given	27.4	300 K, 30 Bar	[10]
MOF-74	MOF-74	Direct carbonization (MOF acts as template and precursor)	2495	Not given	3.4	300 K, 1.5 Bar	[10]
Polymer microspheres (GDMA-*co*-MAA)	Melamine (ML)	ML polymerization, carbonization & KOH activation	683	14.5	2.7	298 K, 1 Bar	[11]
Mesoporous Silica (IBN-9)	Furfuryl Alcohol & p-diaminobenzene	Mixing precursors & templates, drying, carbonization & activation	890	13	10.5	298 K, 8 Bar	[12]
Mesoporous silica (SBA-15) spheres	Ethylenediamine & carbon tetrachloride	Mixing, polymerization & carbonization	550	17.8	2.9	298 K, 1 ~Bar	[13]
Sol-gel method*	Polyaniline (PANi)	PANi polymerization (hydrogel) and freeze-drying (xerogel), carbonization and KOH activation	4196	0.55	28.3	298 K, 30 Bar	[14]
Sol-gel method*	Resorcinol & Formaldehyde (RF)	RF polymerization and air-drying (aerogel), carbonization	1521	Not given	3.0	298 K, 1 Bar	[15]
Temperature induced phase separation (TIPS)*	Polyacrylonitrile (PAN)	Carbonization & CO_2 activation	2501	1.8	10.6	298 K, 3 Bar	[16]
DMSO Ice-crystals	Polyacrylonitrile (PAN)	This work (IT-AC50)	1049	14.9	16.1	298 K, 10 Bar	This Work
DMSO Ice-crystals	Polyacrylonitrile (PAN)	This work (IT-AC50)	1049	14.9	3.2	298 K ~1 Bar	This Work

* Not a templating method but included for comparison

Table S2 H_2 adsorption capacities of various templated carbons published in the literature

Template	Precursor	Method	BET SSA ($m^2 g^{-1}$)	H_2 Adsorption (wt. %)	Conditions	Ref.
Zeolite Y	Acetonitrile	CVD, post-activation w. KOH	3064	2.6	77 K, 1 Bar	[17]
Zeolite β	Acetonitrile	CVD	3150	2.6	77 K, 1 Bar	[18]
Zeolite 13X	Acetonitrile	CVD	1589	1.6	77 K, 1 Bar	[19]
Zeolite Y	Acetonitrile	CVD	1825	2.0	77K, 1 Bar	[19]
Zeolite Y	Propylene	CVD	2117	2.0	77K, 1 Bar	[20]
Mesoporous Silica (MCM-48)	Sucrose	Aqueous impregnation & carbonization	2390	3.5	77K, 1 Bar	[21]
Mesoporous Silica (MCM-48)	Sucrose	Aqueous impregnation & carbonization	1646	2.7	77K, 60 Bar	[22]
Mesoporous Silica (KIT-6)	Polycarbosilane	Organic impregnation & carbonization	2914	3.0	77 K, 135 Bar	[23]
Mesoporous Silica (SBA-15)	Sucrose	Aqueous impregnation, carbonization & CO_2 activation	2749	2.3	77 K, 1 Bar	[24]
Colloidal Silica	Sucrose	Aerosol drying & carbonization	1995	2.0	77 K, 1.1 Bar	[25]
MOF (IRMOF-1)	MOF (IRMOF-1)	Direct carbonization (MOF acts as template and precursor)	3447	3.3	77 K, 1 Bar	[26]
ZIF-8	ZIF-8	Direct carbonization (ZIF acts as template and precursor) & KOH activation	2437	2.6	77 K, ~1 Bar	[9]
Hypercrosslinked porous polymer (COP)	Hypercrosslinked porous polymer (COP)	Direct carbonization & KOH activation	2189	2.6	77 K, 1 Bar	[6]
Sol-gel method*	Resorcinol & Formaldehyde (RF)	RF polymerization and air-drying (aerogel), carbonization	1980	4.3	77 K, 20 Bar	[15]
DMSO Ice-crystals	Polyacrylonitrile (PAN)	This Work (IT-ACMAX)	2206	2.7	77 K, 1.2 Bar	This work

* Not a templating method but included for comparison

References for Table S1 and Table S2

[1] G.-P. Hao, W.-C. Li, D. Qian, G.-H. Wang, W.-P. Zhang, T. Zhang, A.-Q. Wang, F. Schüth, H.-J. Bongard, and A.-H. Lu, Structurally Designed Synthesis of Mechanically Stable Poly(benzoxazine-co-resol)-Based Porous Carbon Monoliths and Their Application as High-Performance CO_2 Capture Sorbents, *J. Am. Chem. Soc.*, 2011, **133**, 11378–11388.

[2] J. Yu, M. Guo, F. Muhammad, A. Wang, F. Zhang, Q. Li, and G. Zhu, One-pot synthesis of highly ordered nitrogen-containing mesoporous carbon with resorcinol–urea–formaldehyde resin for CO_2 capture, *Carbon,* 2014, **69**, 502–514.

[3] J. Wei, D. Zhou, Z. Sun, Y. Deng, Y. Xia, and D. Zhao, A Controllable Synthesis of Rich Nitrogen-Doped Ordered Mesoporous Carbon for CO_2 Capture and Supercapacitors, *Adv. Funct. Mater.*, 2013, **23**, 2322–2328.

[4] J. W. F. To, J. He, J. Mei, R. Haghpanah, Z. Chen, T. Kurosawa, S. Chen, W.-G. Bae, L. Pan, J. B.-H. Tok, J. Wilcox, and Z. Bao, Hierarchical N-Doped Carbon as CO_2 Adsorbent with High CO_2 Selectivity from Rationally Designed Polypyrrole Precursor, *J. Am. Chem. Soc.*, 2016, **138**, 1001–1009.

[5] B. Ashourirad, A. K. Sekizkardes, S. Altarawneh, and H. M. El-Kaderi, Exceptional Gas Adsorption Properties by Nitrogen-Doped Porous Carbons Derived from Benzimidazole-Linked Polymers, *Chem. Mater.*, 2015, **27**, 1349–1358.

[6] A. Modak and A. Bhaumik, Porous carbon derived via KOH activation of a hypercrosslinked porous organic polymer for efficient CO_2, CH_4, H_2 adsorptions and high CO_2/N_2 selectivity, *J. Solid State Chem.*, 2015, **232**, 157–162.

[7] L. Wang and R. T. Yang, Significantly Increased CO_2 Adsorption Performance of Nanostructured Templated Carbon by Tuning Surface Area and Nitrogen Doping, *J. Phys. Chem. C*, 2012, **116**, 1099–1106.

[8] Y. Xia, R. Mokaya, G. S. Walker, and Y. Zhu, Superior CO_2 Adsorption Capacity on N-doped, High-Surface-Area, Microporous Carbons Templated from Zeolite, *Adv. Energy Mater.*, 2011, **1**, 678–683.

[9] Q. Wang, W. Xia, W. Guo, L. An, D. Xia, and R. Zou, Functional Zeolitic-Imidazolate-Framework-Templated Porous Carbon Materials for CO_2 Capture and Enhanced Capacitors, *Chem. - An Asian J.*, 2013, **8**, 1879–1885.

[10] G. Srinivas, V. Krungleviciute, Z.-X. Guo, and T. Yildirim, Exceptional CO_2 capture in a hierarchically porous carbon with simultaneous high surface area and pore volume, *Energy Environ. Sci.*, 2014, **7**, 335–342.

[11] D. Li, Y. Chen, M. Zheng, H. Zhao, Y. Zhao, and Z. Sun, Hierarchically Structured Porous Nitrogen-Doped Carbon for Highly Selective CO_2 Capture, *ACS Sustain. Chem. Eng.*, 2016, **4**, 298–304.

[12] Y. Zhao, L. Zhao, K. X. Yao, Y. Yang, Q. Zhang, and Y. Han, Novel porous carbon materials with ultrahigh nitrogen contents for selective CO_2 capture, *J. Mater. Chem.*, 2012, **22**, 19726.

[13] Q. Li, J. Yang, D. Feng, Z. Wu, Q. Wu, S. S. Park, C.-S. Ha, and D. Zhao, Facile synthesis of porous carbon nitride spheres with hierarchical three-dimensional mesostructures for CO_2 capture, *Nano Res.*, 2010, **3**, 632–642.

[14] J. He, J. W. F. To, P. C. Psarras, H. Yan, T. Atkinson, R. T. Holmes, D. Nordlund, Z. Bao, and J. Wilcox, Tunable Polyaniline-Based Porous Carbon with Ultrahigh Surface Area for CO_2 Capture at Elevated Pressure, *Adv. Energy Mater.*, 2016, **6**, 1502491.

[15] C. Robertson and R. Mokaya, Microporous activated carbon aerogels via a simple subcritical drying route for CO_2 capture and hydrogen storage, *Micropor. Mesopor.Mater.*, 2013, **179**, 151–156.

[16] M. Nandi, K. Okada, A. Dutta, A. Bhaumik, J. Maruyama, D. Derks, and H. Uyama, Unprecedented CO_2 uptake over highly porous N-doped activated carbon monoliths prepared by physical activation, *Chem. Commun.*, 2012, **48**, 10283–10285.

[17] M. Sevilla, N. Alam, and R. Mokaya, Enhancement of Hydrogen Storage Capacity of Zeolite-Templated Carbons by Chemical Activation, *J. Phys. Chem. C*, 2010, **114**, 11314–11319.

[18] Z. Yang, Y. Xia, and R. Mokaya, Enhanced Hydrogen Storage Capacity of High Surface Area Zeolite-like Carbon Materials, *J. Am. Chem. Soc.*, 2007, **129**, 1673–1679.

[19] Z. Yang, Y. Xia, X. Sun, and R. Mokaya, Preparation and hydrogen storage properties of zeolite-templated carbon materials nanocast via chemical vapor deposition: effect of the zeolite template and nitrogen doping., *J. Phys. Chem. B*, 2006, **110**, 18424–31.

[20] L. Chen, R. K. Singh, and P. Webley, Synthesis, characterization and hydrogen storage properties of microporous carbons templated by cation exchanged forms of zeolite Y with propylene and butylene as carbon precursors, *Micropor.Mesopor. Mater.*, 2007, **102**, 159–170.

[21] R. Gadiou, S.-E. Saadallah, T. Piquero, P. David, J. Parmentier, and C. Vix-Guterl, The influence of textural properties on the adsorption of hydrogen on ordered nanostructured carbons, *Microporous Mesoporous Mater.*, 2005, **79**, 121–128.

[22] E. Terrés, B. Panella, T. Hayashi, Y. A. Kim, M. Endo, J. M. Dominguez, M. Hirscher, H. Terrones, and M. Terrones, Hydrogen storage in spherical nanoporous carbons, *Chem. Phys. Lett.*, 2005, **403**, 363–366.

[23] M. Oschatz, E. Kockrick, M. Rose, L. Borchardt, N. Klein, I. Senkovska, T. Freudenberg, Y. Korenblit, G. Yushin, and S. Kaskel, A cubic ordered, mesoporous carbide-derived carbon for gas and energy storage applications, *Carbon*, 2010, **48**, 3987–3992.

[24] K. Xia, Q. Gao, C. Wu, S. Song, and M. Ruan, Activation, characterization and hydrogen storage properties of the mesoporous carbon CMK-3, *Carbon,* 2007, **45**, 1989–1996.

[25] Q. Hu, Y. Lu, and G. P. Meisner, Preparation of Nanoporous Carbon Particles and Their Cryogenic Hydrogen Storage Capacities, *J. Phys. Chem. C*, 2008, **112**, 1516–1523.

[26] S. J. Yang, T. Kim, J. H. Im, Y. S. Kim, K. Lee, H. Jung, and C. R. Park, MOF-Derived Hierarchically Porous Carbon with Exceptional Porosity and Hydrogen Storage Capacity, *Chem. Mater.*, 2012, **24**, 464–470.